# Modular Transcriptional Activity Characterizes the Initiation and Progression of Autoimmune Encephalomyelitis[1]

**Sergio E. Baranzini,[2]* Claude C. A. Bernard,† and Jorge R. Oksenberg***

**Murine experimental autoimmune encephalomyelitis is a well-established model that recapitulates many clinical and physiopathological aspects of multiple sclerosis (MS). An important conceptual development in the understanding of both experimental autoimmune encephalomyelitis and MS pathogenesis has been the compartmentalization of the mechanistic process into two distinct but overlapping and connected phases, inflammatory and neurodegenerative. However, the dynamics of CNS transcriptional changes that underlie the development and regression of the phenotype are not well understood. Our report presents the first high frequency longitudinal study looking at the earliest transcriptional changes in the CNS of NOD mice immunized with myelin oligodendrocyte glycoprotein 35–55 in CFA. Microarray-based gene expression profiling and histopathological analysis were performed from spinal cord samples obtained at 13 time points around the first clinical symptom (every other day until day 11 and every day onward until day 19 postimmunization). Advanced statistics and data-mining algorithms were used to identify expression signatures that correlated with disease stage and histological profiles. Discrete phases of neuroinflammation were accompanied by distinctive expression signatures, in which altered immune to neural gene expression ratios were observed. By using high frequency gene expression analysis we captured expression profiles that were characteristic of the transition from innate to adaptive immune response in this experimental paradigm between days 11 and 12 postimmunization. Our study demonstrates the utility of large-scale transcriptional studies and advanced data mining to decipher complex biological processes such as those involved in MS and other neurodegenerative disoders.** *The Journal of Immunology,* **2005, 174: 7412–7422.**

Chronic autoimmune diseases like multiple sclerosis (MS)[3] develop over the course of months or years without exhibiting any observable phenotype. By following patterns of gene expression over time in suitable and well-controlled experimental models, it should be possible to identify early pathogenic mechanisms that precede symptoms and to unravel regulatory events undetectable at the clinical or pathological level. Experimental autoimmune encephalomyelitis (EAE) can be induced in a variety of animal species, including nonhuman primates, by active immunization with myelin proteins or their peptide derivatives, as well as by adoptive transfer of activated $CD4^+$ T cells specific for myelin components (1–6). The encephalitogenic challenge compromises blood-brain barrier (BBB) integrity and produces CNS inflammation and neurodegeneration leading to neurologic disease. Ataxia and paralysis occurs first in the tail and hind limbs, and progressive deterioration later affects the forelimbs, eventually causing death. From all available EAE murine models, the one induced by myelin oligodendrocyte glycoprotein $(MOG)_{35–55}$ in the NOD background is perhaps the most adequate for a time-controlled experiment, in which one relies on synchronicity and dynamics of clinical symptoms. Furthermore, this model results in severe chronic relapsing disease, resembling a characteristic population of MS patients (7). Although clearly some differences exist with the human disease, this model shares common clinical, histological, immunologic, and genetic features. A large body of experimental data firmly established a role for Th1 cells, B cells, microglia, and their soluble products as initiators and regulators of the CNS inflammatory response in both MS and EAE (8, 9). However the full array of molecular mechanisms effectors and/or regulators of myelin injury and axonal loss remain uncertain.

The past few years have seen real progress in the development of large-scale genetic approaches to study complex biological systems. The careful and methodic mining of gene expression data, for example, could lead to the identification of coregulated genes and to the characterization of networks that underlie specific cellular process. This multiplex organization is what ultimately defines the function, and therefore, the phenotype. A number of recent reports have described transcriptional profiles in the CNS of rodent EAE, helping in defining the molecular fingerprint of the demyelinating process (10–16). However, most of these studies focused on recounting cross-sectional expression patterns associated with the peak of clinical symptoms. We report a high quality, longitudinal expression dataset that enabled the formulation of more precise mechanistic models of EAE pathogenesis. Spinal cords were collected from NOD mice for detailed histological and DNA microarray analysis before immunization with $MOG_{35–55}$ peptide and at 13 subsequent time points encompassing the first clinical attack and recovery phase. The results show abnormal patterns of gene expression in the affected tissue very early in the disease process, preceding the detection of inflammation. As the disease progresses, there is a strong correlation between gene expression, histological findings, and the clinical phenotype.

*Department of Neurology, School of Medicine, University of California, San Francisco, CA 94143; and †Neuroimmunology Laboratory, School of Biochemistry and Genetics, LaTrobe University, Bundoora, Victoria, Australia

Received for publication January 11, 2005. Accepted for publication March 11, 2005.

The costs of publication of this article were defrayed in part by the payment of page charges. This article must therefore be hereby marked *advertisement* in accordance with 18 U.S.C. Section 1734 solely to indicate this fact.

[1] This work was supported by the Wadsworth Foundation and the National Health and Medical Research Council of Australia.

[2] Address correspondence and reprint requests to Dr. Sergio E. Baranzini, Department of Neurology, University of California, School of Medicine, 513 Parnassus Avenue, Room S-256, San Francisco, CA 94143-0435. E-mail address: sebaran@cgl.ucsf.edu

[3] Abbreviations used in this paper: MS, multiple sclerosis; EAE, experimental autoimmune encephalomyelitis; BBB, blood-brain barrier; MOG, myelin oligodendrocyte glycoprotein; PCA, principal component analysis.



0022-1767/05/$02.00

## Materials and Methods

### *Mice*

NOD mice (8- to 13-wk-old) were bred and maintained at the La Trobe University Central Animal House (Bundoora, Melbourne, Australia). All experiments were conducted in accordance with the Australian code of practice for the care and use of animals for scientific purposes (National Health and Medical Research Council 1997), after approval by the La Trobe University Animal Ethics committee (Melbourne, Australia).

### *Animal immunization and EAE clinical scoring*

A total of 124 female mice were divided into three groups. The immunized group comprised 91 mice injected s.c. into the lower flanks with 200 $\mu$g of $MOG_{35–55}$ peptide (MEVGWYRSPFSRVVHLYRNGK; Auspep) emulsified in CFA containing 4 mg/ml *Mycobacterium tuberculosis* (Difco). An i.v. injection of 350 ng of *Bordetella pertussis* toxin was administered both immediately thereafter and 48 h later. The 26 mice in the control group were injected with adjuvant and pertussis toxin only. The seven animals used for the baseline group (time, day 0) were naive, not injected mice. Mice were monitored daily for signs of EAE. Clinical scores were graded as 0, no clinical sign; 0.5, tail weakness; l, limp tail; 2, limp tail and impaired righting reflex; and 3, hind limb paralysis. No scores higher than 3 were observed during the course of our experiments. Intermediate scores were assigned if neurologic signs were milder than typically observed.

### *Sample collection*

Except for the seven naive animals from the baseline group, nine animals (seven from the EAE and two from the control group) were sacrificed (at the same time of the day) at each of 13 time points after immunization, which are detailed as days 3, 5, 7, 9, 11, 12, 13, 14, 15, 16, 17, 18, and 19 postimmunization. At baseline and at each time point after $MOG_{35–55}$ injection, three animals were immediately perfused with 4% paraformaldehyde in 0.1 M phosphate buffer, and their brains and entire spinal cords were removed and processed for histological staining. Brain and spinal cords from the remaining four animals of the immunized and from the two control groups were dissected, immersed in RNAlater (Ambion), and frozen at −20°C.

### *Histology*

Segments of fixed brain, cerebellum, and spinal cord were embedded in paraffin. Sections were stained with H&E, Luxol fast blue, and Bielschowsky silver for evidence of inflammation, demyelination, and axonal damage, respectively. Twenty-six to 30 sagittal sections per mouse were examined. Semiquantitative histological evaluation for inflammation and demyelination was performed and scored in a blind fashion as follow: 0, no inflammation; 1, cellular infiltrate only in the perivascular areas and meninges; 2, mild cellular infiltrate in parenchyma; 3, moderate cellular infiltrate in parenchyma; and 4, severe and diffuse cellular infiltrate in parenchyma. The myelin breakdown was assessed and scored as follows: 0, no demyelination; 1, mild demyelination; 2, moderate demyelination; and 3, severe demyelination (17).

### *RNA purification and microarray probe synthesis*

Spinal cords were removed from RNAlater and homogenized in TRIzol (Invitrogen Life Technologies) using an electric homogenizer. After resuspending the final RNA pellet in water, samples were repurified using the RNeasy kit (Qiagen). cDNA was synthesized from 15 $\mu$g of total RNA using Superscript II RT (Invitrogen Life Technologies) and a modified dNTP mix containing dUTP. Samples were hydrolyzed by adding 10 $\mu$l of 0.1 N NaOH, neutralized with 25 $\mu$l of 1 M HEPES, and precipitated with 3 M sodium acetate and ethanol. Resuspension in 0.05 M sodium bicarbonate was followed by 1 h incubation with either *N*-hydroxysuccinimide ester Cy3 or Cy5 fluorescent dyes (Amersham Biosciences). Probes were quenched by the addition of 4 M hydroxylamine and neutralized with 100 mM sodium acetate. Final probe cleanup was conducted using the QIAQuick PCR purification kit (Qiagen). We followed a common reference design in which each Cy3-labeled spinal cord probe was combined with a Cy5-labeled probe derived from a pool of brain and spleen RNA. Hybridization onto glass slides containing 18,240 spotted 60- to 70-mer oligonucleotides, followed by washing and scanning was performed at the Gladstone microarray core facility at the University of California (San Francisco, CA).

### *Microarray data analysis*

A stringent quality control check was performed for each microarray based on the diagnostic plots generated by the marrayTools package of Bioconductor (⟨www.biocondutor.org⟩). Specifically, statistical tests were conducted to verify that: 1) the normalized ratio of intensities (M) for the positive and negative control genes was similar; 2) the normalized product of intensities (A) for the positive and negative control genes was different; 3) the spatial distribution of normalized M values for all genes in the array was similar; 4) the spatial distribution of normalized product of intensity values was similar; and 5) the mean signal to noise ratio for all probes for each color exceeded a previously set threshold of 1.4. Arrays were considered of high quality if no more than one of these tests failed. Based on our quality control check, seven arrays were eliminated from further analysis. Raw data are imported into BRB-Array Tools (Biometric Research Branch, National Institutes of Health, Bethesda, MD) and subsequently filtered for flagged spots and Lowess normalized. All class comparison tests were performed in BRB-Array Tools. For statistical significance of all class comparisons, we performed the F test with a nominal value of $p = 0.001$. In addition, random permutations of the class labels (i.e., which experiments correspond to which classes) were conducted. For each random permutation, the F tests were recomputed for each gene. The proportion of the random permutations resulting in as many genes significant at the 0.001 level as were found in comparing the true class labels were then computed. This value $p = 0.001$ provides a global test of whether the expression profiles in the classes are different, and is the one reported throughout this study. This method also allows for controlling for the false discovery rate. All clustering and principal component analyses (PCA) were done in GeneLinker Platinum (Predictive Patterns).

### *Gene ontology analysis*

For each gene ontology group we computed the number of genes represented on the microarray in that group and the statistical significance $p_i$ value for each gene in the group. These $p$ values reflect differential expression among classes and were computed based on random variance F tests (18). A sample number of genes is randomly selected from genes represented on the array and the summary statistic is computed for those random samples. The significance level associated with the gene ontology category is the proportion of the random samples, giving as large a value of the summary statistic as found in the actual number of genes of the gene ontology category. We considered a gene ontology category significantly differentially regulated if either significance level was $<0.005$. We considered all gene ontology categories with between 5 and 100 genes represented on the array. Because gene ontology is inherently redundant, some of the categories were overlapping.

### *Analysis of neural vs immune genes*

To establish the origin and function of each of the genes contained in the array, its Unigene record was examined and the source tissues from which the cDNA libraries derived were recorded. A gene was classified as either neural or immune if at least 20% of the source cDNA libraries contained one or more of a list of keywords previously defined. Based on this algorithm, genes represented in the microarray were classified as immune (11%), neural (15%), both (8%), or none (66%). Although admittedly this algorithm generates some false negatives (66% of the genes belong to the "none" category), we gain specificity in the "immune" and "neural" categories. As a result, these categories contain transcripts classified with very high confidence. To express the ratios, the number of UP to DOWN genes was calculated for each EAE stage and for each origin (immune or neural). If UP<DOWN, then the ratio was transformed to $-(\text{UP/DOWN})^{-1}$ to keep the absolute value of the ratio $>1$ and thus facilitate visualization.

### *Real-time PCR*

Three genes showing differential expression in different EAE stages were selected for validation by real-time PCR by TaqMan in 50 samples each, thus totaling 150 reactions. Primers and probes were obtained through Assays-on-Demand (Applied Biosystems) and reactions were conducted in an ABI HT-7900 following manufacturer's instructions.

## Results

### *Study design*

Ninety-one female NOD mice were immunized with $MOG_{35–55}$ (immunized group), and seven animals were sacrificed at baseline and at each of 13 subsequent time points (days 3 to 19 postimmunization) as detailed in *Materials and Methods*. At each time point, spinal cords from four mice were removed and processed for DNA microarray analysis, whereas the CNS of the remaining three animals were formalin-fixed and prepared for histological staining. As a control group, another 26 mice were injected with CFA and

pertussis toxin only (referred to as adjuvant) and two animals from this group were sacrificed at the same 13 time points. For the baseline group, seven animals were sacrificed before immunization (three for histology and four for RNA profiling).

*EAE variable dynamics*

All mice were scored daily throughout the duration of the experiment. Although all animals were genetically identical, immunized at the same time with the same pool of reagents, and kept under the same environmental conditions, we observed slight variability in disease onset and progression, possibly due to stochastic factors inherent to inconsistent food intake, stress, or other behavioral conditions preceding immunization. Interestingly, a plasma proteomic profile of the four naive animals analyzed at baseline shows a moderate degree of heterogeneity (data not shown), an unexpected finding given the homogeneous genetic background and controlled conditions under which this experiment was conducted. To control for this variability, animals were segregated into groups with similar disease kinetics until the time of euthanasia (Table I). Based on such grouping, we were able to classify each sample into six distinct EAE stages: 1, before immunization (baseline, day 0 postimmunization); 2, presymptomatic or before onset of EAE (days 3–12 postimmunization); 3, early EAE (days 13–15 postimmunization); 4, peak EAE (day 17 postimmunization); 5, early recovery (day 16 postimmunization); and 6, late recovery (day 18 postimmunization). A group of four animals (killed at day 19 postimmunization) did not get sick and were excluded from subsequent experiments.

All histological samples were stained with H&E to assess inflammation, whereas selected samples (those from time point day 6 onward) were stained with Luxol fast blue (demyelination) and Bielschowsky silver (axonal damage) (Fig. 1). Extensive inflammatory lesions, characterized by mononuclear inflammatory cells and severe edema (Fig. 1) were observed in the forebrain, pons, medulla, cerebellum, and spinal cord starting at day 12 postimmunization and were particularly abundant in the cerebellum and spinal cord. Luxol fast blue and Bielschowsky silver staining also revealed myelin loss and axonal injury, particularly around the injured tissue and more predominantly in the cerebellum and spinal cord. However these were only observed at a later stage of the disease, around day 18 postimmunization.

*Transcriptional profiling*

For a full analysis of this dataset we mainly performed two type of comparisons. First, a cumulative expression profiling was studied to assess the magnitude of the molecular changes associated with progression through each of the six EAE stages described above. We also used this strategy to compare the early changes evidenced in spinal cords in immunized and control mice before any signs of inflammation or disease. Second, stage-specific gene expression profiles were performed at each of the six clinically defined stages to better characterize their molecular signatures. To validate microarray results, the expression of three genes (*IL-10Ra*, *Ltf*, and *Mpz*) in 50 samples was also assessed by quantitative PCR. An average correlation coefficient of 0.8 was observed between the two methods (data not shown).

***Cumulative expression profiling in immunized and control mice.*** To evaluate the extent and complexity of the molecular changes taking place in the CNS upon immunization with $MOG_{35–55}$, we first identified and tabulated the cumulative number of genes differentially expressed (relative to baseline) in the immunized and control groups. We observed a sustained and time-dependent increase in the number of differentially expressed genes in the immunized group with 63 genes identified before clinical onset increasing to 1687 genes in the late recovery stage (F test, $p < 0.001$) (Fig. 2). This is not an unexpected finding because it mainly reflects the entire process of massive recruitment of immune cells into the CNS and possibly, its response to such process. The transcript with the most dramatic change along all time points was that of myeloperoxidase (*Mpo*), a heme protein present in the azurophil granules of neutrophils that generates reactive intermediates promoting lipid peroxidation. Together with other neutrophil-specific genes (*Ltf*, defensins), *Mpo* up-regulation was detected before pathological signs of inflammation and even in the absence of MOG peptide, suggesting that this initial increase responds to the recruitment of neutrophils as part of the innate immune response to *Mycobacterium*. As the disease progressed beyond the early EAE time point, a dramatic increase (up to 41.7-fold in peak EAE, $p = 0.0001$) in this transcript was seen in immunized animals when compared with levels in animals at baseline. This trend continued on to later time points.

Interestingly, when gene expression in the spinal cords of control animals was compared with baseline, 34 genes were differentially expressed by as early as day 12 postimmunization (equivalent to the time point before EAE in the immunized animals). At the 0.001 significance level used, only 17 genes would be expected to be called significant by chance suggesting that at least half of these represent genuine significant differences. Given that 11% of the genes in our microarrays were strictly immune-related (see *Materials and Methods*), fewer than 4 immune-related genes would be expected if all categories of genes had the same probability of being dysregulated (i.e., because 11% of the genes in the array are immune-related, false positive hits should follow this "default" distribution). However, 8 of 34 genes (23%) were found to be immune-related, indicating a statistically significant increase of genes in this category ($p < 0.028$, $\chi^2$). Moreover, a detailed evaluation of the genes in this list provides further evidence for their biological role in adjuvant-related damage (Table II). Furthermore, an uprising trend was observed with a peak of 79 genes differentially expressed at early and peak EAE stages (Fig. 2). Taken together, these results suggest that the expression of these genes may be reflecting the nonspecific response to the adjuvant.

Table I. *Sample grouping and differentially expressed genes*

| EAE Stage | Time[a] (dpi) | No. of Samples | No. of Genes Differentially Expressed (Cumulative) | No. of Genes Differentially Expressed against T0 ($p < 0.001$) | No. of Genes Stage-Specific |
|---|---|---|---|---|---|
| Baseline | T0 | 4 | N/A | N/A | N/A |
| BE | T1–T6 | 21 | 63 | 63 (18) | 30 (8) |
| EE | T7–T9 | 12 | 442 | 319 (150) | 125 (41) |
| PE | T11 | 4 | 1210 | 528 (333) | 396 (42) |
| ER | T10 | 4 | 1435 | 498 (311) | 233 (24) |
| LR | T12 | 4 | 1687 | 251 (113) | 11 (1) |

[a] Time at euthanasia (in days postimmunization).

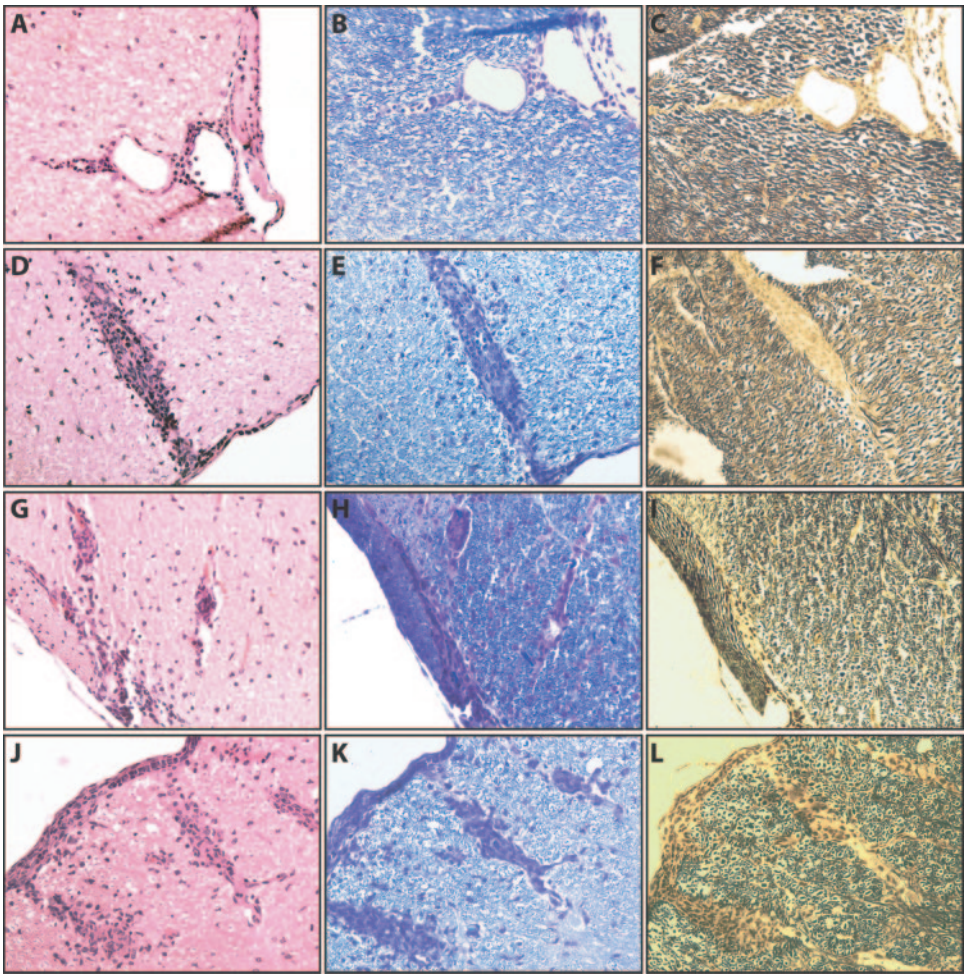


**FIGURE 1.** Histopathology of the spinal cords of NOD mice during the progression of clinical EAE. Representative sections taken at days 12 (*A–C*), 15 (*D–F*), 17 (*G–I*), and 18 (*J–L*) postimmunization were stained with H&E for lymphocyte infiltration (*A*, *D*, *G*, and *J*), Luxol fast blue for myelin (*B*, *E*, *H*, and *K*), and Bielschowsky silver staining for axons (*C*, *F*, *I*, and *L*). *A*, Small typical inflammatory infiltrations in the spinal cord at day 12 postimmunization (magnification, ×400). Note the few lymphocytes adhering to a blood vessel. *B* and *C*, Luxol fast blue and Bielschowsky silver staining of adjacent sections, respectively, showing the absence of myelin loss and the integrity of axons (magnification, ×400). Although the number and size of inflammatory lesions increased as the disease progressed, demyelination and axonal damage was only evident at day 18 postimmunization (*K* and *L*).

***Stage-specific gene expression profiles.*** With the aim of determining whether a gene expression signature existed for each of the EAE stages defined in our classification, we performed a PCA with the 1687 differentially expressed across all stages of EAE (Fig. 3) (a list of these genes is provided in supplemental table 1.[4]). Notably, the tested specimens segregated according to their corresponding clinical stage with those from disease peak (Fig. 3, red) and before EAE onset (Fig. 3, yellow) occupying opposite regions of the PCA three-dimensional space, as they display the most different patterns of expression. Samples corresponding to the early EAE group (Fig. 3, orange) spanned a wider region (mainly along the horizontal axis) denoting molecular heterogeneity en route to a full EAE inflammatory profile. Samples from recovery stages (early and late recovery) lay closer to those from the peak EAE stage but their distribution (specially late recovery samples) was less homogeneous than that seen for peak EAE or before EAE stages. This again suggests that different expression profiles are consistent with the observed phenotype.

### *Adjuvant-induced gene expression changes*

As described earlier, the expression of 34 genes was changed significantly in controls by day 12 postimmunization (Fig. 2). Interestingly, 12 of these genes were up-regulated with a very similar magnitude in the immunized group, suggesting an early common response to the nonspecific stimulus produced by adjuvants (Table II). These included genes with known early activity during the immune response such as uteroglobin-related protein 2 (*Utgrp2*), neutrophilic granule protein (*Ngp*), synaptotagmin 2 (*Syt2*), haptoglobin (*Hp*), phospholipase $D_1$ (*Pld1*), and tissue inhibitor of matrix metalloproteinase 2 (*Timp2*).

The early, nonspecific up-regulation of *Ngp* transcripts suggests the presence of neutrophils, one of the earliest cells of the innate immune system in arriving at sites of inflammation. By liberating the contents of their granules and secretory vesicles, neutrophils play an important role in migration across the endothelium (19). In the context of EAE, neutrophils may contribute to the sensitization of the basal lamina of blood vessels thus priming BBB disruption, a necessary step in the induction of EAE. Our data is consistent with a previous report describing significant delay and in some cases total prevention of clinical EAE by Ab-mediated depletion of peripheral blood polymorphonuclear cells (20). The presence of *Timp2* and *Hp* among this group of genes strengthens this hypothesis because matrix metalloproteinases and their inhibitors are known to play an early role in BBB damage (21–23). Also, Hp polymers have been previously identified as a sensitive indicator of BBB permeability (24, 25). Collectively, these findings indicate that the integrity of the BBB is significantly compromised before inflammation arises, and provide evidence that expression changes can be detected in the CNS even in the absence of an Ag-specific encephalitogenic stimulus.

### *Early MOG-induced gene expression changes*

Sixty-three genes were identified by F test when all samples up to day 12 postimmunization (before onset of EAE group) were compared against baseline (Table I, Fig. 2). We then considered each

[4] The online version of this article contains supplemental material.

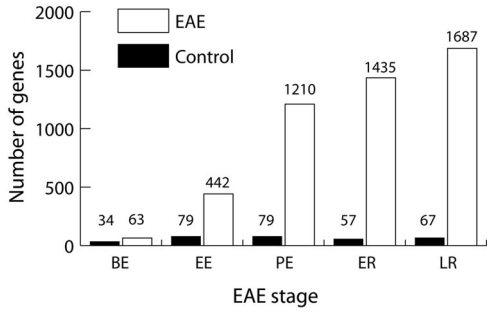


**FIGURE 2.** Cumulative gene expression changes in EAE and controls. The number of genes differentially expressed in spinal cords after immunization with MOG (□) or adjuvant alone (■).

time point comprising this group individually and found 162 genes differentially expressed (F test, $p < 0.001$). In this analysis we found that as early as day 11 postimmunization, several transcripts associated with the innate immune response were identified (*C6*, *Cd36*, *Cmkar4*, *Gp49b*, *Tgtp, Mona*, *Cd3*). Also, the expression of genes with cell adhesion (*Mmp8*, *Ddr2*, *Ceacam1*) or neural (*Chrm4*, *Kcnmb4*, *Nnat*, *Otog*) functions was detected at this stage (complete list available upon request). Interestingly, 1 day later (day 12 postimmunization) several genes were identified that are normally associated with the early stages of the adaptive immune response (*Saa3*, *Cd52*, *Ifit1*, and small inducible cytokines *A2*, *A12*, *B9*, *B10*, and *B13*) (complete list available upon request). These results suggest that in $MOG_{35–55}$-immunized NOD mice, the transition from a predominantly innate into adaptive immune response may occur between 11 and 12 days after immunization.

*Expression changes during clinical EAE*

Having characterized the changes occurring before onset of EAE, we next set out to discover expression profiles accompanying the clinical course of EAE. To that end, we compared the gene expression signature of each stage against baseline. As initially suggested by the relative spread in the PCA plot (Fig. 3), there is considerable overlapping of differentially expressed genes in several categories, particularly among early, peak, and early recovery EAE stages (Fig. 4). To minimize this variability, and using the spread in PCA three-dimensional space as a guide, we selected for further analysis only those samples with similar PCA profile for each EAE stage (Fig. 3, dotted line). A graphic representation of all the differentially expressed genes (Fig. 4, columns) for each EAE stage (Fig. 4, rows) is depicted. This strategy resulted in the identification of transcriptional signatures representative of at least three EAE stages. Areas of stage-specific genes in early EAE, peak EAE, and early recovery EAE are distinguished (Fig. 4, yellow boxes). A detailed list of stage-specific EAE genes is provided in supplemental table 2.

Although both neural and immune-derived specific genes were differentially expressed in most stages, we observed an interesting correlation between the direction of expression changes (up or down) and the unique cellular origin (immune or neural) of those transcripts. For this analysis we only considered those genes differentially expressed in each specific EAE stage. The origin of each transcript (immune or neural) was traced by examination of the Unigene database. We developed an algorithm to classify the origin of genes based on the number of cDNA libraries in which a given gene was present and which of those were derived from immune or neural related organs (see *Materials and Methods*). Interestingly, the sum of immune and neural differentially expressed genes does not change dramatically in any of the EAE stages when compared with their overall (default) distribution in the microarray (11% immune, 15% neural). However, an increase of 15% for immune genes calls was seen in the peak EAE stage (26% of all differentially expressed genes in peak EAE were immune-related). This can be explained by the (counterbalancing) reduction in differentially expressed genes of neural origin in this stage (from 15 to 8%). Except for very early or late stages in the disease, immune-related genes were mainly up-regulated and neural genes were mainly down-regulated. Apart from gene regulation, a possible explanation for this finding is that as more immune cells gain access to the CNS, their relative RNA contribution per mass of neural tissue increases. Conversely, the increased cell death induced by the active inflammatory process may cause a sizeable reduction in the amount of neural-specific transcripts. In the early EAE stage, a similar proportion of neural and immune genes are differentially regulated (12 and 17%, respectively). However, although the ratio of UP to DOWN for immune genes in this stage was 1.95, we observed a strong bias toward down-regulation of neural genes (almost 6-fold, Fig. 4*C*). In contrast, in the peak EAE stage, this ratio is clearly reversed as there are many more immune genes up-regulated (24.3-fold) than there are neural genes down-regulated (1.6-fold). Although this trend is maintained in the early recovery EAE stage, the UP to DOWN ratio for immune genes is smaller (13.8-fold), implying that inflammation is less severe than in the peak EAE stage, at least in molecular terms. These findings suggest that there is a CNS response to inflammation manifested in early stages of EAE, possibly contributing to the subsequent, transient resolution of the disease.

Finally, a gene ontology-oriented analysis was conducted involving the previously selected samples from all EAE stages. By analyzing gene ontology groups, rather than individual genes, we were able to reduce the number of tests conducted. In addition, this grouping strategy allowed us to identify biologically related genes thus reinforcing the results obtained at the single gene level. A total of 162 gene ontologies were significant at the 0.005 level using a permutation-based random variance F test (see *Materials and Methods*). Of these, we manually eliminated the redundant entries and selected only those gene ontology entries belonging to the main class "biological process". This yielded 41 gene ontology entries that were subsequently clustered (Pearson correlation) to not only test their expression homogeneity but also to better follow their temporal behavior (Fig. 5). Using a correlation coefficient of 0.7 as a cutoff value, the gene ontology entries were segregated into four well-defined clusters with interesting dynamics. Cluster 1 shows a maximum at the peak EAE stage of at least twice the values seen at baseline and does not change significantly thereafter. This profile is consistent with that seen for inflammation as scored by (blinded) pathological examination (Fig. 5*B*, purple bars). Cluster 2 shows a similar profile to that of cluster 1, although the observed changes with respect to baseline are more moderate. This correlates well with the clinical scores (Fig. 5*B*, magenta bars). Cluster 3 progressively increases up to 80% above baseline levels at the peak EAE stage and subsequently falls to almost baseline levels. Cluster 4 shows a negative trend as the disease progresses, indicating down-regulation of their corresponding genes. Interestingly, this cluster contains eight genes involved in locomotory behavior including ephrin, ephrin receptor, otogelin, and a voltage-gated sodium channel. Also in this cluster are 79 genes involved in potassium transport including ionotropic glutamate receptors and several voltage-gated potassium channels. The prompt down-regulation of this group of genes suggests that neural damage is a very early feature of EAE and their subsequent decline toward later stages might be responsible for the clinical phenotype.

Table II. *Differentially expressed genes before EAE onset*[a]

| EAE | | | | | Controls | | | | |
|---|---|---|---|---|---|---|---|---|---|
| GenBank Accession No. | Gene Symbol | Fold Change[b] | *p* Value | Category | GenBank Accession No. | Gene Symbol | Fold Change[b] | *p* Value | Category |
| **NM_054037** | **Utgrp2** | **4.90** | **2.E-04** | Immune | **NM_054037** | **Utgrp2-pending** | **5.24** | **4.E-06** | **Immune** |
| **NM_008694** | **Ngp** | **4.13** | **2.E-05** | Neither | **AK003422** | **RIKEN clone 1110004H09** | **4.22** | **3.E-04** | **Neither** |
| **AK003422** | **RIKEN clone 1110004H09** | **3.86** | **8.E-04** | Neither | **NM_008694** | **Ngp** | **3.76** | **2.E-05** | **Neither** |
| **NM_017370** | **Hp** | **3.19** | **6.E-04** | Immune | **NM_017370** | **Hp** | **3.07** | **4.E-06** | **Immune** |
| **NM_009307** | **Syt2** | **2.84** | **2.E-04** | Neural | NM_011291 | Rpl7 | 3.05 | 8.E-05 | Neither |
| **BC017616** | **RIKEN gene 2310045I24** | **2.34** | **4.E-05** | Neither | NM_008530 | Ly6f | 3.03 | 6.E-05 | Neither |
| **NM_033149** | **B3galt5** | **2.22** | **5.E-05** | Both | **NM_009307** | **Syt2** | **2.83** | **6.E-04** | **Neural** |
| **AK006096** | **RIKEN gene 1700018O18** | **2.20** | **4.E-06** | Neither | NM_009242 | Sparc | 2.76 | 3.E-04 | Neither |
| **U87868** | **Pld1** | **2.02** | **4.E-04** | Neither | NM_008611 | Mmp8 | 2.65 | 4.E-04 | Immune |
| **AK007978** | **RIKEN gene 1810073O08** | **1.99** | **7.E-05** | Immune | BC019150 | Hoxd9 | 2.63 | 6.E-04 | Neither |
| **NM_011594** | **Timp2** | **1.99** | **4.E-05** | Neither | NM_009510 | Vil2 | 2.53 | 3.E-04 | Neither |
| **NM_009459** | **Ube2h** | **1.92** | **2.E-04** | Neither | NM_023142 | Arpc1b | 2.48 | 2.E-05 | Immune |
| NM_010003 | Cyp2c39 | 2.87 | 7.E-05 | Neither | NM_010184 | Fcer1a | 2.29 | 3.E-04 | Immune |
| BC007144 | EST C80816 | 2.76 | 6.E-06 | Neither | BC005615 | RIKEN gene 1190003K14 | 2.26 | 3.E-04 | Neither |
| NM_010456 | Hoxa9 | 2.54 | 8.E-05 | Neither | **BC017616** | **RIKEN gene 2310045I24** | **2.24** | **2.E-04** | **Neither** |
| AF416641 | Ipas | 2.23 | 5.E-04 | Neither | NM_009841 | Cd14 | 2.24 | 1.E-04 | Immune |
| BC021916 | S100a11 | 2.22 | 5.E-04 | Neither | **NM_009459** | **Ube2h** | **2.22** | **3.E-04** | **Neither** |
| NM_007407 | Adcyap1r1 | 2.14 | 2.E-04 | Neural | **U87868** | **Pld1** | **2.13** | **7.E-04** | **Neither** |
| NM_019499 | Mad2l1 | 2.13 | 7.E-04 | Neither | AK008492 | RIKEN gene 2010300F21 | 2.13 | 2.E-05 | Immune |
| NM_011638 | Trfr | 2.08 | 2.E-04 | Neither | **NM_033149** | **B3galt5** | **2.10** | **3.E-04** | **Both** |
| AK016188 | RIKEN gene 4930562C03 | 2.00 | 2.E-04 | Neither | **AK006096** | **RIKEN gene 1700018O18** | **2.06** | **2.E-04** | **Neither** |
| NM_013568 | Kcna6 | 1.99 | 3.E-04 | Neither | AK006458 | RIKEN gene 1700028G04 | 2.00 | 5.E-04 | Neither |
| NM_011828 | Hs2st1 | 1.99 | 5.E-04 | Neural | **AK007978** | **RIKEN gene 1810073O08** | **1.97** | **7.E-04** | **Immune** |
| NM_010795 | Mgat3 | 1.97 | 2.E-04 | Neither | BC021513 | IMAGE clone 5351756 | 1.90 | 1.E-04 | Neither |
| AY007594 | Tcf20 | 1.95 | 2.E-04 | Neither | **NM_011594** | **Timp2** | **1.89** | **5.E-04** | **Neither** |
| NM_030743 | Zfp313 | 1.91 | 2.E-04 | Neither | BC005786 | IMAGE clone 2811511 | 1.89 | 1.E-04 | Neither |
| NM_007920 | Elf1 | 1.90 | 8.E-04 | Neither | NM_007646 | Cd38 | 1.84 | 6.E-04 | Neither |
| NM_011941 | Jnkbp1 | 1.85 | 8.E-04 | Neither | NM_008402 | Itgav | 1.80 | 9.E-04 | Neither |
| NM_013599 | Mmp9 | 1.83 | 3.E-04 | Both | AK011539 | RIKEN gene 2610024M03 | 1.78 | 6.E-04 | Neither |
| AK007108 | RIKEN gene 1700101I19 | 1.81 | 7.E-04 | Neither | NM_023058 | Pkmyt1 | 0.55 | 8.E-04 | Neither |
| NM_030561 | Gene MGC:7550 | 1.79 | 9.E-04 | Neither | AK002767 | RIKEN gene 0610037B23 | 0.52 | 3.E-04 | Neither |
| NM_025509 | RIKEN gene 2310008M10 | 1.76 | 4.E-04 | Neither | BC012256 | IMAGE clone 4205488 | 0.47 | 8.E-04 | Neither |
| NM_020269 | Kcnj10 | 1.76 | 6.E-04 | Neural | AK015714 | RIKEN gene 4930506C21 | 0.46 | 1.E-04 | Neither |
| NM_011929 | Clcn6 | 1.63 | 8.E-04 | Both | AK015562 | RIKEN clone 4930473A02 | 0.44 | 5.E-04 | Neither |
| AF033663 | Prpk | 1.59 | 9.E-04 | Both | | | | | |
| NM_025450 | Mprs17 | 0.65 | 8.E-04 | Neither | | | | | |
| AK013199 | RIKEN gene 2810429P03 | 0.65 | 8.E-04 | Neither | | | | | |
| AK004009 | RIKEN clone 1110031M01 | 0.65 | 7.E-04 | Neither | | | | | |
| NM_028513 | RIKEN gene 1700052K15 | 0.63 | 6.E-04 | Neither | | | | | |
| NM_021452 | Kcnmb4 | 0.62 | 9.E-05 | Neither | | | | | |
| NM_028003 | RIKEN gene 2310042P20 | 0.61 | 3.E-04 | Neural | | | | | |
| NM_010134 | En2 | 0.60 | 7.E-04 | Neural | | | | | |
| NM_009203 | Slc22al2 | 0.60 | 9.E-04 | Immune | | | | | |
| NM_025708 | RIKEN gene 4432406C05 | 0.59 | 6.E-04 | Both | | | | | |
| BC009098 | EST AI042819 | 0.59 | 1.E-04 | Neither | | | | | |
| BC022666 | RIKEN gene 1110007F23 | 0.58 | 9.E-04 | Neither | | | | | |
| BC003858 | RIKEN gene 1300019I21 | 0.58 | 9.E-04 | Neither | | | | | |
| NM_017399 | Fabp1 | 0.58 | 3.E-04 | Neither | | | | | |
| AK018267 | RIKEN gene 6330591G05 | 0.58 | 4.E-04 | Neither | | | | | |
| BC010821 | IMAGE clone 4218355 | 0.57 | 2.E-04 | Neither | | | | | |
| AK012812 | RIKEN gene 2810025M15 | 0.56 | 1.E-04 | Neither | | | | | |
| NM_010281 | Ggh | 0.56 | 2.E-04 | Neither | | | | | |
| BC003195 | IMAGE clone 3586067 | 0.56 | 2.E-04 | Neither | | | | | |
| BC007167 | Nxph3 | 0.55 | 4.E-04 | Neither | | | | | |
| NM_054084 | Calcb | 0.53 | 3.E-04 | Neither | | | | | |
| M16360 | Mup5 | 0.53 | 7.E-05 | Neither | | | | | |
| NM_008718 | Npas1 | 0.52 | 9.E-05 | Neither | | | | | |
| NM_030687 | Slc21a5 | 0.51 | 5.E-04 | Neural | | | | | |
| NM_008803 | Pde8a | 0.51 | 7.E-04 | Neural | | | | | |
| X83932 | Ryr1 | 0.49 | 9.E-05 | Neither | | | | | |
| AK018679 | RIKEN gene 9130415E20 | 0.49 | 2.E-04 | Neither | | | | | |
| NM_007809 | Cyp17 | 0.43 | 1.E-04 | Neither | | | | | |
| NM_009394 | Tncs | 0.33 | 4.E-04 | Neither | | | | | |

[a] The first 12 genes in the immunized animals were also differentially expressed in the controls (shown in bold). Horizontal lines separate up-regulated from down-regulated genes in each list.

[b] Fold change with respect to baseline expression.

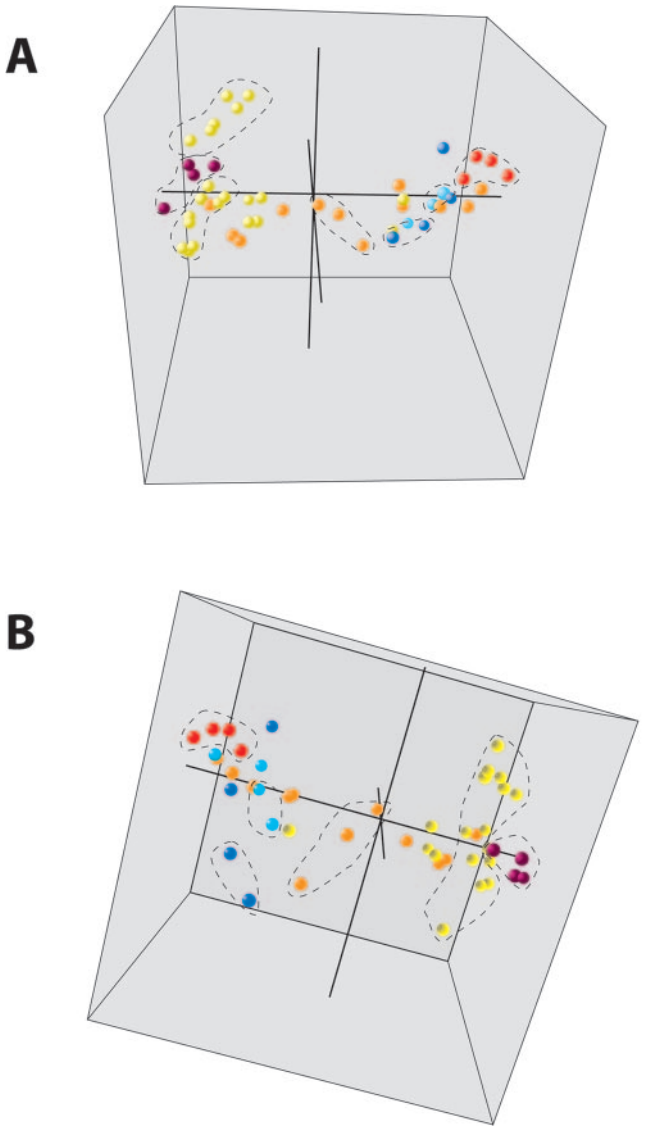


**FIGURE 3.** PCA with the 1687 most variable genes in EAE. Samples are layered onto the three-dimensional space based on their gene expression patterns. A view from two different angles is shown to highlight the separation across different EAE stages. There is a marked agreement between the phenotypic (clinical score) and molecular (gene expression) classifications. Each circle represents a single RNA sample and their color indicates the EAE stage: baseline (fuchsia); before EAE (BE, yellow); early EAE (EE, orange); peak EAE (PE, red); early recovery (ER, light blue); and late recovery (LR, dark blue). Selected samples for stage-specific (dotted line) expression analyses are indicated.

## Discussion

We describe in this study the molecular and pathological dynamics observed in spinal cords of NOD mice immunized with $MOG_{35-55}$. From the several murine models available, we chose the one that in our hands showed the most efficient induction rate, a synchronized disease onset, a chronic relapsing course, and histopathological signs consistent with the human disease. Due to the controlled conditions and short time course duration of our experiment (19 days in total), we deemed that the spontaneous diabetic pathology characteristic of these mice would not interfere with the results reported. To further account for this, our experimental design included animals of the same age that only received adjuvant, but that were sacrificed at the same time points than their immunized littermates, thus allowing for adjusted comparisons directed to address this potential concern.

Changes in gene expression and pathological scores were systematically assessed at 13 time points during the first 19 days after immunization either with adjuvant alone or with the encephalitogenic MOG-containing emulsion. To our knowledge, this is the first study that attempts to capture the molecular events leading to EAE in such a high frequency, time course fashion. Our work uncovers four important aspects of EAE that could also shed light into the pathogenesis of MS: 1) strong unspecific peripheral immune activation induced by adjuvant results in transcriptional changes in the CNS. Our data support a prominent role for neutrophils during the effector phase of EAE; 2) upon immunization, substantial gene expression changes in spinal cords are detectable before histological evidence of inflammation. Transcriptional patterns consistent with a transition from an innate to an adaptive immune response were detected in CNS between days 11 and 12 postimmunization; 3) discrete phases of neurologic disease are accompanied by distinctive expression signatures. Their full characterization may reveal potential therapeutic targets; 4) down-regulation of genes involved in potassium transport including ionotropic glutamate receptors and several voltage-gated potassium channels further support the observation that neural damage is a very early feature of EAE.

We report that even in the absence of specific encephalitogenic stimulus, gene expression changes can be detected in the CNS (i.e., in adjuvant-injected animals). We identified up to 79 genes that were differentially expressed after adjuvant injection (Fig. 2). Approximately one-third of these genes were down-regulated and included molecules mainly expressed in brain such *Tieg*, *Mix1*, *Nrgn*, and *Slc6a4*, suggesting a neural response to a peripheral insult. Up-regulated genes mostly reflect the activity of proteins involved in lymphocyte adhesion, transendothelial migration, and disruption of the BBB such as Vil2, Mmp8, and Hp (21, 24–26). Also among up-regulated transcripts was *Hoxd9*, a gene previously found in synoviocytes from rheumatoid arthritis patients, *CD52*, a panlymphocyte Ag, and *Mal-1*, a T cell differentiation protein. Taken together these findings suggest that even in the absence of encephalitogenic stimulus, the BBB is damaged and immune-related transcripts can be found in the CNS. The presence of neutrophil-specific transcripts (*Ngp*, *Mpo*, *Ltf*) in the CNS indicates that these cells transmigrated the vascular endothelium for which previous rolling, tethering, and adhesion are necessary steps (27). It has been previously shown that polymorphonuclear cells are critical during the effector phase of EAE, as depleting these cells after day 8 postimmunization sensibly reduced disease incidence (20). Our results provide molecular evidence that adjuvants alone are sufficient to facilitate vascular permeability by a process involving the transcription of several genes.

Alteration of gene expression patterns in the CNS is a very early feature of MOG-induced EAE, naturally anticipating both clinical symptoms and, more interestingly, pathological evidence of inflammation. The presence of transcripts with immunologic, adhesion, or neural functions can be detected by as early as day 11 postimmunization, several days before the onset of EAE. One of these genes (*C6*) is a complement component, whose absence has been shown to ameliorate the symptoms of EAE possibly due to its critical role during formation of the membrane attack complex (28). Another transcript with elevated expression was *Cd36*, a multiligand scavenger receptor expressed by the cell of the monocyte/macrophage lineage (including microglia) that plays important roles in cell attachment, motility, and proliferation as well as atherosclerosis, inflammation, thrombosis, TGF-$\beta$ activation, neurite

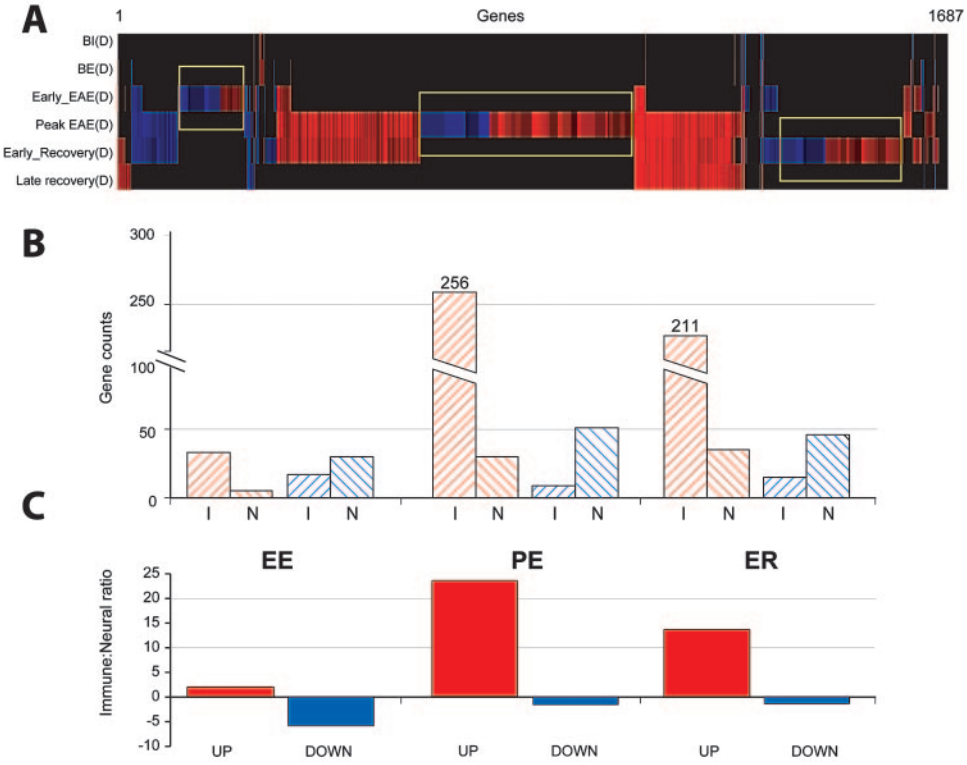


**FIGURE 4.** EAE stage-specific gene expression analysis. *A*, For each stage, only those genes called differentially expressed after false discovery rate correction are included. Up-regulated genes are indicated in increasingly brighter shades of red, while down-regulated genes are depicted in increasingly brighter shades of blue. Genes differentially expressed (yellow boxes) exclusively in each of three characteristic EAE stages are highlighted: early EAE (EE), peak EAE (PE), and early recovery (ER). *B*, The number of genes from immune (I) or neural (N) origin that were differentially up-regulated (red hatched bars) or down-regulated (blue hatched bars) in early, peak, and early recovery EAE stages. *C*, The ratio of up-regulated (red) vs down-regulated (blue) genes (UP/DOWN) from immune and neural origin is compared in early, peak, and early recovery EAE stages. If UP<DOWN, the ratio was transformed to $-(\text{UP/DOWN})^{-1}$ (see *Materials and Methods* for details).

outgrowth, and angiogenesis (29). Statins, an effective cholesterol-lowering family of drugs, are highly effective in treating EAE, and clinical trials in MS patients are currently under way (30, 31). Surprisingly, it has been recently shown that statins are potent activators of *Cd36* transcription and translation in human monocytes (32). Also, Tgtp, a macrophage and T cell GTPase with antiviral functions, was early up-regulated. Expression of *Tgtp* has been shown to be selectively induced by IFN-$\gamma$ and in some cases by IFN-$\alpha$/IFN-$\beta$ or bacterial LPS (33). This induction pattern also implicates *Tgtp* as part of the innate defense of cells to infection and its early expression in EAE temporally correlates with that of *Mpo*, *Ltf*, and *Ngp*.

Although a large number of genes were significantly regulated during peak disease, we focused on those with the largest differential expression. The gene coding for Fyn binding protein (*Fyb*), was among the most elevated at the peak EAE stage. Fyb is an adaptor molecule that mediates positive regulation of T cell activation and integrin adhesion (34). Among the down-regulated genes in this category is *Epha5*, whose product is required for a normal topographic guidance of growing axons in the CNS. Also, Rho GDP dissociation inhibitor $\gamma$ (also known as *RIP2*) was significantly down-regulated in peak EAE. *RIP2* is a stress-inducible upstream modulator of procaspase-1 apoptotic activation and its decreased expression may reflect an active mechanism to reduce neuronal cell death (35). In addition, caspase-1 is an activator of IL-1b and a reduced expression might contribute to a negative regulation of the inflammatory process (36).

Among the most expressed transcripts characteristic of the early recovery phase is *uromodulin* (3.3-fold, $p = 0.0003$), a urine-derived inhibitor of IL-1. There is evidence suggesting that this glycoprotein (present in the urine of pregnant women) is potent inhibitor of IL-1-induced thymocyte proliferation and human lymphocyte activation. Notably, *IL-1b* is also differentially up-regulated in this stage (3-fold, $p = 0.0002$), suggesting an active regulatory mechanism. CD44, transcripts coding for a hyaluronic acid-binding protein and the molecular receptor for osteopontin (Opn), were also up-regulated in the early recovery EAE stage (4.4-fold, $p = 0.0004$). CD44 has been linked to the inflammatory process by its ability to recruit lymphocytes, and *OPN* transcripts have been found increased in inflammatory lesions of EAE and MS (16). One of the genes with reduced expression in the early recovery phase was somatostatin receptor 2 (*Smstr2*), known to participate as part of an immunomodulatory axis in response to chronic inflammation. Somatostatin down-modulates a number of immune functions, among others lymphocyte proliferation, Ig production and the release of proinflammatory cytokines such as IFN-$\gamma$. Given that somatostatin levels modulate the expression of its receptors, it is possible that the reduced expression of *Smstr2* reflects a regulatory mechanism in response to increased levels of somatostatin, as an attempt to control inflammation in the early recovery phase of EAE.

Potential therapeutic targets. Several of the genes found to be differentially expressed, particularly in early stages of the disease, have been targeted for therapeutic intervention in both mice and humans. Among these targets *Mpo*, *CD52*, lactotransferrin (*Ltf*), *CD44*, *Smstr2*, and phospholipase $A_2$ (*Pla2*) are of particular interest. Paradoxically, although *Mpo* serves as a major enzymatic catalyst possibly perpetuating inflammation, its absence has been shown to enhance inflammation and to have a detrimental role in

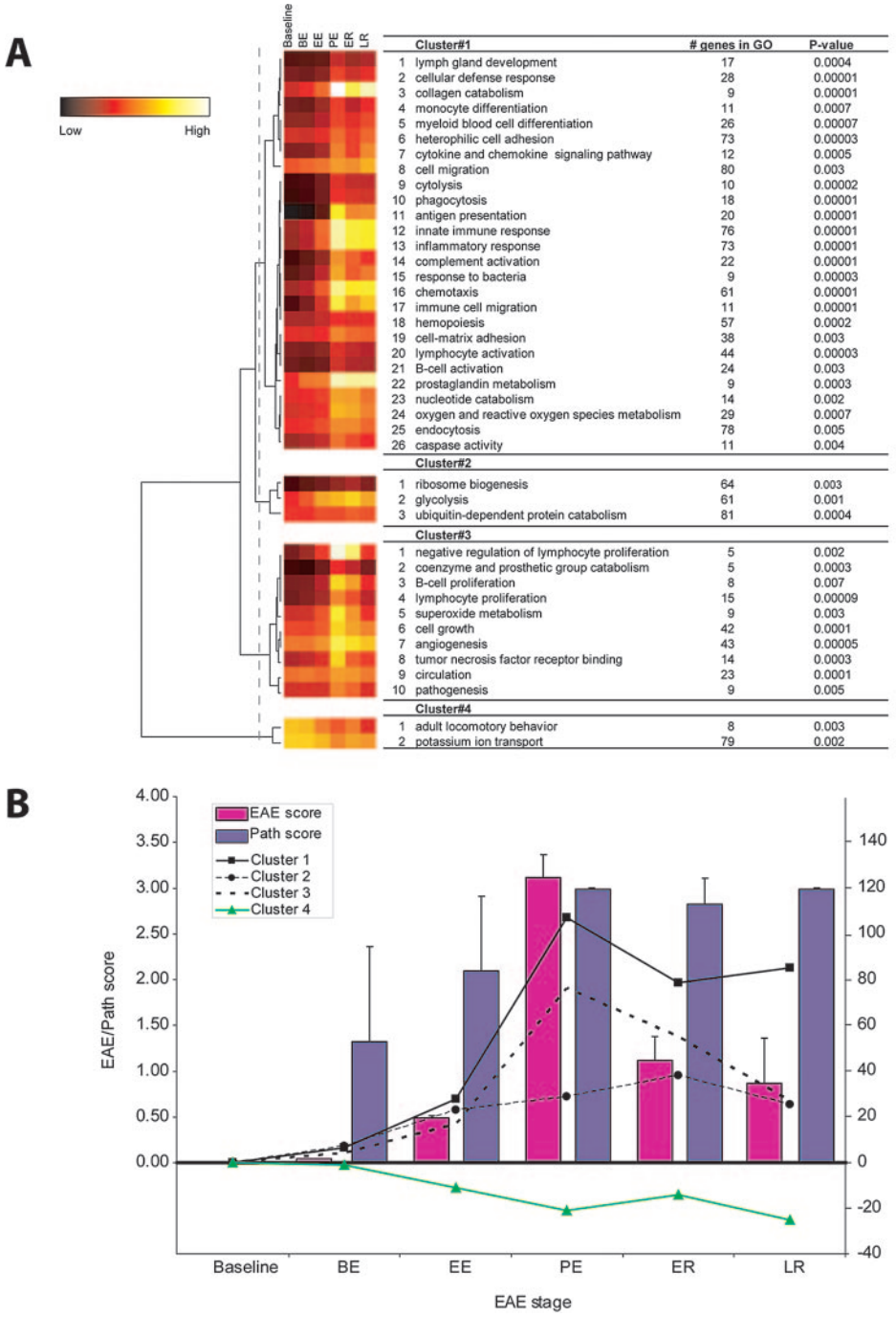


| | Cluster#1 | # genes in GO | P-value |
|---|---|---|---|
| 1 | lymph gland development | 17 | 0.0004 |
| 2 | cellular defense response | 28 | 0.00001 |
| 3 | collagen catabolism | 9 | 0.00001 |
| 4 | monocyte differentiation | 11 | 0.0007 |
| 5 | myeloid blood cell differentiation | 26 | 0.00007 |
| 6 | heterophilic cell adhesion | 73 | 0.00003 |
| 7 | cytokine and chemokine signaling pathway | 12 | 0.0005 |
| 8 | cell migration | 80 | 0.003 |
| 9 | cytolysis | 10 | 0.00002 |
| 10 | phagocytosis | 18 | 0.00001 |
| 11 | antigen presentation | 20 | 0.00001 |
| 12 | innate immune response | 76 | 0.00001 |
| 13 | inflammatory response | 73 | 0.00001 |
| 14 | complement activation | 22 | 0.00001 |
| 15 | response to bacteria | 9 | 0.00003 |
| 16 | chemotaxis | 61 | 0.00001 |
| 17 | immune cell migration | 11 | 0.00001 |
| 18 | hemopoiesis | 57 | 0.0002 |
| 19 | cell-matrix adhesion | 38 | 0.003 |
| 20 | lymphocyte activation | 44 | 0.00003 |
| 21 | B-cell activation | 24 | 0.003 |
| 22 | prostaglandin metabolism | 9 | 0.0003 |
| 23 | nucleotide catabolism | 14 | 0.002 |
| 24 | oxygen and reactive oxygen species metabolism | 29 | 0.0007 |
| 25 | endocytosis | 78 | 0.005 |
| 26 | caspase activity | 11 | 0.004 |
| | **Cluster#2** | | |
| 1 | ribosome biogenesis | 64 | 0.003 |
| 2 | glycolysis | 61 | 0.001 |
| 3 | ubiquitin-dependent protein catabolism | 81 | 0.0004 |
| | **Cluster#3** | | |
| 1 | negative regulation of lymphocyte proliferation | 5 | 0.002 |
| 2 | coenzyme and prosthetic group catabolism | 5 | 0.0003 |
| 3 | B-cell proliferation | 8 | 0.007 |
| 4 | lymphocyte proliferation | 15 | 0.00009 |
| 5 | superoxide metabolism | 9 | 0.003 |
| 6 | cell growth | 42 | 0.0001 |
| 7 | angiogenesis | 43 | 0.00005 |
| 8 | tumor necrosis factor receptor binding | 14 | 0.0003 |
| 9 | circulation | 23 | 0.0001 |
| 10 | pathogenesis | 9 | 0.005 |
| | **Cluster#4** | | |
| 1 | adult locomotory behavior | 8 | 0.003 |
| 2 | potassium ion transport | 79 | 0.002 |

**FIGURE 5.** Clusters of gene ontology characteristic of EAE clinical and pathological stages. *A*, Forty-one gene ontology classes discriminating among EAE scores were subjected to hierarchical clustering (Pearson correlation), and using 0.7 as a cutoff (gray dotted line) four clusters emerged, each of which displays a characteristic profile across different EAE stages. The table lists each ontology along with the number of corresponding genes and the *p* value for the permutation-based test (Fisher statistic). *B*, To better follow their temporal behavior, the intensity of expression for each of the four clusters was averaged and plotted against each EAE stage. The *y* axis (*left*) of the chart measures clinical score (EAE score, magenta) and pathological score (Path score, purple) for each EAE stage. The *y* axis (*right*) indicates the percentage variation of gene ontology clusters compared with baseline levels. Cluster 1 (solid line, ■); cluster 2 (broken line, ●); cluster 3 (broken line); and cluster 4 (green solid line, green triangles).

EAE (37, 38). This is analogous to the controversial role of the inducible form of NO synthase in EAE, for which both pathogenic and disease-suppressive functions have been described (39, 40).

*CD52* was found in our study to be up-regulated in adjuvant-treated animals. As an attempt to reduce the inflammatory reaction affecting the brain of MS patients, a therapeutic approach was conducted using monoclonal anti-*CD52* Ab (Campath 1H) as a lymphocyte-depleting agent (41). Although radiological and clinical markers of disease activity were significantly decreased for at least 18 mo after treatment, one-third of patients developed Abs against the thyrotropin receptor and autoimmune hyperthyroidism. It was concluded that Campath-1H causes the immune response to change from a Th1 to a Th2 phenotype, suppressing MS disease activity, but permitting the generation of Ab-mediated thyroid autoimmunity.

Lactotransferrin, a molecule known to be up-regulated in response to acute inflammation, was among the genes highly expressed in several stages of EAE. Data from several biochemical and pharmacological studies indicate that free radicals participate in the pathogenesis of MS and EAE, and iron has been implicated as the catalyst leading to their formation (42). In the brain, this redoxactive element may facilitate the reduction of hydrogen peroxide ($H_2O_2$) to highly cytotoxic hydroxyl radicals. In this context, increased expression of the iron-binding *Ltf* might be reflecting a regulatory mechanism to reduce the amount of free iron in affected white matter. Interestingly, oral administration of Ltf has been found to significantly reduce inflammation and nociception in an arthritis model through down-regulation of *TNF-α* and up-regulation of *IL-10* (43, 44).

Oral administration of Ltf inhibits NO-mediated inflammation by several different mechanisms (43–47). It is worth noting that exacerbations in MS are reduced during the pregnancy period in which Ltf expression levels are maximal (48). These observations suggest that Ltf could open a therapeutic venue for MS patients.

Anti-*CD44* Abs have been shown to prevent or dramatically alleviate inflammation in experimental models of autoimmunity (49–52). These Abs may block interaction of CD44 with its extracellular matrix ligand, hyaluronan, an interaction that plays a critical role in a number of biological functions, including cell migration, tumorigenesis, metastasis, and regulation of immune responses. In addition, the CD44 ligand OPN has been shown to be a critical regulator of the Th1 proinflammatory phenotype observed in EAE. Furthermore, $OPN^{-/-}$ mice showed a significantly milder EAE course than their wild-type littermates (16). Thus, it seems that CD44 contributes both to the activation and sustainability of the immune response. Therapeutic strategies aimed at blocking this molecule with such a multiplicity of functions should be considered in MS.

We found the *Smstr2* down-regulated in the early recovery stage of EAE. Given the plethora of regulatory functions associated to somatostatin, particularly during inflammation, pharmacological modulation with this peptide or its receptors should perhaps be attempted to restore homeostatic balance. Interestingly, it has been recently shown that systemic or local treatment with somatostatin or some of its analogues is beneficial in a number of in vivo models of autoimmune disease and chronic inflammation (53).

In summary, high frequency longitudinal transcriptional profiling of neuroinflammation in model animals allowed us to characterize the earliest pathogenic events associated with EAE, including a transitional phase between the innate and adaptive immune responses. Well-demarcated expression patterns characteristic of specific stages of EAE were identified, and the prominent role for neutrophils during the effector phase of EAE was confirmed. Also, we detected an imbalance in the expression of immune vs neural-related genes that correlated with disease progression. Interestingly, a CNS transcriptional response was evident even in the absence of specific encephalitogenic challenges. Finally, down-regulation of genes involved in potassium transport including ionotropic glutamate receptors and several voltage-gated potassium channels further support the observation that neural damage is a very early feature of EAE (54). In MS patients different disease types may exist, which are relatively stable in individual patients throughout the course of the disease (55, 56). Thus, it would be reasonable to search for refined animal models that accurately mimic each of them. Our methodology could serve as an example for future characterization of other body compartments (brain, peripheral organs, blood) and experimental models resembling different subtypes or stages of the disease. The comprehensive analysis of these cellular transcriptional programs in the CNS should provide the molecular fingerprint of the neuropathologic process and help identify the complete array of disease genes.

## Acknowledgments

We thank Althea Stillman, Jonathan McQualter, and Tara Karnezis for their technical help with the initial experiments and valuable discussions during preparation of this manuscript. We also thank the anonymous referees for a thorough revision of the manuscript.

## Disclosures

The authors have no financial conflict of interest.

## References

1. Zamvil, S., P. Nelson, J. Trotter, D. Mitchell, R. Knobler, R. Fritz, and L. Steinman. 1985. T-cell clones specific for myelin basic protein induce chronic relapsing paralysis and demyelination. *Nature* 317: 355–358.
2. Zamvil, S. S., D. J. Mitchell, A. C. Moore, K. Kitamura, L. Steinman, and J. B. Rothbard. 1986. T-cell epitope of the autoantigen myelin basic protein that induces encephalomyelitis. *Nature* 324: 258–260.
3. Swanborg, R. H. 1995. Experimental autoimmune encephalomyelitis in rodents as a model for human demyelinating disease. *Clin. Immunol. Immunopathol.* 77: 4–13.
4. McRae, B. L., M. K. Kennedy, L. J. Tan, M. C. Dal Canto, K. S. Picha, and S. D. Miller. 1992. Induction of active and adoptive relapsing experimental autoimmune encephalomyelitis (EAE) using an encephalitogenic epitope of proteolipid protein. *J. Neuroimmunol.* 38: 229–240.
5. Encinas, J. A., M. B. Lees, R. A. Sobel, C. Symonowicz, J. M. Greer, C. L. Shovlin, H. L. Weiner, C. E. Seidman, J. G. Seidman, and V. K. Kuchroo. 1996. Genetic analysis of susceptibility to experimental autoimmune encephalomyelitis in a cross between SJL/J and B10.S mice. *J. Immunol.* 157: 2186–2192.
6. Johns, T. G., N. Kerlero de Rosbo, K. K. Menon, S. Abo, M. F. Gonzales, and C. C. Bernard. 1995. Myelin oligodendrocyte glycoprotein induces a demyelinating encephalomyelitis resembling multiple sclerosis. *J. Immunol.* 154: 5536–5541.
7. Bernard, C. C., T. G. Johns, A. Slavin, M. Ichikawa, C. Ewing, J. Liu, and J. Bettadapura. 1997. Myelin oligodendrocyte glycoprotein: a novel candidate autoantigen in multiple sclerosis. *J. Mol. Med.* 75: 77–88.
8. Hartung, H. P., and P. Rieckmann. 1997. Pathogenesis of immune-mediated demyelination in the CNS. *J. Neural Transm. (Suppl.* 50): 173–181.
9. Kennedy, K. J., and W. J. Karpus. 1999. Role of chemokines in the regulation of Th1/Th2 and autoimmune encephalomyelitis. *J. Clin. Immunol.* 19: 273–279.
10. Mix, E., S. Ibrahim, J. Pahnke, D. Koczan, C. Sina, T. Bottcher, H. J. Thiesen, and A. Rolfs. 2004. Gene-expression profiling of the early stages of MOG-induced EAE proves EAE-resistance as an active process. *J. Neuroimmunol.* 151: 158–170.
11. Niculescu, T., S. Weerth, L. Soane, F. Niculescu, V. Rus, C. S. Raine, M. L. Shin, and H. Rus. 2003. Effects of membrane attack complex of complement on apoptosis in experimental autoimmune encephalomyelitis. *Ann. NY Acad. Sci.* 1010: 530–533.
12. Matejuk, A., C. Hopke, J. Dwyer, S. Subramanian, R. E. Jones, D. N. Bourdette, A. A. Vandenbark, and H. Offner. 2003. CNS gene expression pattern associated with spontaneous experimental autoimmune encephalomyelitis. *J. Neurosci. Res.* 73: 667–678.
13. Carmody, R. J., B. Hilliard, K. Maguschak, L. A. Chodosh, and Y. H. Chen. 2002. Genomic scale profiling of autoimmune inflammation in the central nervous system: the nervous response to inflammation. *J. Neuroimmunol.* 133: 95–107.
14. Whitney, L. W., S. K. Ludwin, H. F. McFarland, and W. E. Biddison. 2001. Microarray analysis of gene expression in multiple sclerosis and EAE identifies 5-lipoxygenase as a component of inflammatory lesions. *J. Neuroimmunol.* 121: 40–48.
15. Lock, C., G. Hermans, R. Pedotti, A. Brendolan, E. Schadt, H. Garren, A. Langer-Gould, S. Strober, B. Cannella, J. Allard, et al. 2002. Gene-microarray analysis of multiple sclerosis lesions yields new targets validated in autoimmune encephalomyelitis. *Nat. Med.* 8: 500–508.
16. Chabas, D., S. E. Baranzini, D. Mitchell, C. C. A. Bernard, S. R. Rittling, D. T. Denhardt, R. A. Sobel, C. Lock, M. Karpuj, R. Pedotti, et al. 2001. The influence of the proinflammatory cytokine, osteopontin, on autoimmune demyelinating disease. *Science* 294: 1731–1735.
17. Karnezis, T., W. Mandemakers, J. L. McQualter, B. Zheng, P. P. Ho, K. A. Jordan, B. M. Murray, B. Barres, M. Tessier-Lavigne, and C. C. Bernard. 2004. The neurite outgrowth inhibitor Nogo A is involved in autoimmune-mediated demyelination. *Nat. Neurosci.* 7: 736–744.
18. Wright, G. W., and R. M. Simon. 2003. A random variance model for detection of differential gene expression in small microarray experiments. *Bioinformatics* 19: 2448–2455.
19. Borregaard, N., and J. B. Cowland. 1997. Granules of the human neutrophilic polymorphonuclear leukocyte. *Blood* 89: 3503–3521.
20. McColl, S. R., M. A. Staykova, A. Wozniak, S. Fordham, J. Bruce, and D. O. Willenborg. 1998. Treatment with anti-granulocyte antibodies inhibits the effector phase of experimental autoimmune encephalomyelitis. *J. Immunol.* 161: 6421–6426.
21. Leppert, D., S. L. Leib, C. Grygar, K. M. Miller, U. B. Schaad, and G. A. Hollander. 2000. Matrix metalloproteinase (MMP)-8 and MMP-9 in cerebrospinal fluid during bacterial meningitis: association with blood-brain barrier damage and neurological sequelae. *Clin. Infect. Dis.* 31: 80–84.
22. Anthony, D. C., K. M. Miller, S. Fearn, M. J. Townsend, G. Opdenakker, G. M. Wells, J. M. Clements, S. Chandler, A. J. Gearing, and V. H. Perry. 1998. Matrix metalloproteinase expression in an experimentally-induced DTH model of multiple sclerosis in the rat CNS. *J. Neuroimmunol.* 87: 62–72.
23. Lorenzl, S., G. De Pasquale, A. Z. Segal, and M. F. Beal. 2003. Dysregulation of the levels of matrix metalloproteinases and tissue inhibitors of matrix metalloproteinases in the early phase of cerebral ischemia. *Stroke* 34: e37–e38.
24. Rosnowska, M., and W. Cendrowski. 1978. Haptoglobin levels in the serum and the cerebrospinal fluid patients with multiple sclerosis. *Neurol. Neurochir. Pol.* 12: 579–585.
25. Mattila, K. M., T. Pirttila, K. Blennow, A. Wallin, M. Viitanen, and H. Frey. 1994. Altered blood-brain-barrier function in Alzheimer's disease? *Acta Neurol. Scand.* 89: 192–198.

26. Barreiro, O., M. Yanez-Mo, J. M. Serrador, M. C. Montoya, M. Vicente-Manzanares, R. Tejedor, H. Furthmayr, and F. Sanchez-Madrid. 2002. Dynamic interaction of VCAM-1 and ICAM-1 with moesin and ezrin in a novel endothelial docking structure for adherent leukocytes. *J. Cell Biol.* 157: 1233–1245.
27. Berton, G., S. R. Yan, L. Fumagalli, and C. A. Lowell. 1996. Neutrophil activation by adhesion: mechanisms and pathophysiological implications. *Int. J. Clin. Lab. Res.* 26: 160–177.
28. Tran, G. T., S. J. Hodgkinson, N. Carter, M. Killingsworth, S. T. Spicer, and B. M. Hall. 2002. Attenuation of experimental allergic encephalomyelitis in complement component 6-deficient rats is associated with reduced complement C9 deposition, P-selectin expression, and cellular infiltrate in spinal cords. *J. Immunol.* 168: 4293–4300.
29. Febbraio, M., D. P. Hajjar, and R. L. Silverstein. 2001. CD36: a class B scavenger receptor involved in angiogenesis, atherosclerosis, inflammation, and lipid metabolism. *J. Clin. Invest.* 108: 785–791.
30. Youssef, S., O. Stuve, J. C. Patarroyo, P. J. Ruiz, J. L. Radosevich, E. M. Hur, M. Bravo, D. J. Mitchell, R. A. Sobel, L. Steinman, and S. S. Zamvil. 2002. The HMG-CoA reductase inhibitor, atorvastatin, promotes a Th2 bias and reverses paralysis in central nervous system autoimmune disease. *Nature* 420: 78–84.
31. Stuve, O., T. Prod'homme, S. Youssef, S. Dunn, O. Neuhaus, M. Weber, H. P. Hartung, L. Steinman, and S. S. Zamvil. 2004. Statins as potential therapeutic agents in multiple sclerosis. *Curr. Neurol. Neurosci. Rep.* 4: 237–244.
32. Ruiz-Velasco, N., A. Dominguez, and M. A. Vega. 2004. Statins upregulate CD36 expression in human monocytes, an effect strengthened when combined with PPAR-γ ligands putative contribution of Rho GTPases in statin-induced CD36 expression. *Biochem. Pharmacol.* 67: 303–313.
33. Carlow, D. A., S.-J. Teh, and H.-S. Teh. 1998. Specific antiviral activity demonstrated by TGTP, a member of a new family of interferon-induced GTPases. *J. Immunol.* 161: 2348–2355.
34. Griffiths, E. K., C. Krawczyk, Y.-Y. Kong, M. Raab, S. J. Hyduk, D. Bouchard, V. S. Chan, I. Kozieradzki, A. J. Oliveira-Dos-Santos, A. Wakeham, et al. 2001. Positive regulation of T cell activation and integrin adhesion by the adapter Fyb/Slap. *Science* 293: 2260–2263.
35. Zhang, W. H., X. Wang, M. Narayanan, Y. Zhang, C. Huo, J. C. Reed, and R. M. Friedlander. 2003. Fundamental role of the Rip2/caspase-1 pathway in hypoxia and ischemia-induced neuronal cell death. *Proc. Natl. Acad. Sci. USA* 100: 16012–16017.
36. Lamkanfi, M., M. Kalai, X. Saelens, W. Declercq, and P. Vandenabeele. 2004. Caspase-1 activates NF-κB independent of its enzymatic activity. *J. Biol. Chem.* 279: 24785–24793.
37. Brennan, M., A. Gaur, A. Pahuja, A. J. Lusis, and W. F. Reynolds. 2001. Mice lacking myeloperoxidase are more susceptible to experimental autoimmune encephalomyelitis. *J. Neuroimmunol.* 112: 97–105.
38. Milla, C., S. Yang, D. N. Cornfield, M.-L. Brennan, S. L. Hazen, A. Panoskaltsis-Mortari, B. R. Blazar, and I. Y. Haddad. 2004. Myeloperoxidase deficiency enhances inflammation after allogeneic marrow transplantation. *Am. J. Physiol.* 287: L706–L714.
39. Kahl, K. G., J. Zielasek, L. O. Uttenthal, J. Rodrigo, K. V. Toyka, and H. H. Schmidt. 2003. Protective role of the cytokine-inducible isoform of nitric oxide synthase induction and nitrosative stress in experimental autoimmune encephalomyelitis of the DA rat. *J. Neurosci. Res.* 73: 198–205.
40. Giovannoni, G., S. J. Heales, J. M. Land, and E. J. Thompson. 1998. The potential role of nitric oxide in multiple sclerosis. *Mult. Scler.* 4: 212–216.
41. Coles, A. J., M. Wing, S. Smith, F. Coraddu, S. Greer, C. Taylor, A. Weetman, G. Hale, V. K. Chatterjee, H. Waldmann, and A. Compston. 1999. Pulsed monoclonal antibody treatment and autoimmune thyroid disease in multiple sclerosis. *Lancet* 354: 1691–1695.
42. Levine, S. M., and A. Chakrabarty. 2004. The role of iron in the pathogenesis of experimental allergic encephalomyelitis and multiple sclerosis. *Ann. NY Acad. Sci.* 1012: 252–266.
43. Hayashida, K., T. Kaneko, T. Takeuchi, H. Shimizu, K. Ando, and E. Harada. 2004. Oral administration of lactoferrin inhibits inflammation and nociception in rat adjuvant-induced arthritis. *J. Vet. Med. Sci.* 66: 149–154.
44. Guillen, C., I. B. McInnes, D. Vaughan, A. B. Speekenbrink, and J. H. Brock. 2000. The effects of local administration of lactoferrin on inflammation in murine autoimmune and infectious arthritis. *Arthritis Rheum.* 43: 2073–2080.
45. Baveye, S., E. Elass, J. Mazurier, and D. Legrand. 2000. Lactoferrin inhibits the binding of lipopolysaccharides to L-selectin and subsequent production of reactive oxygen species by neutrophils. *FEBS Lett.* 469: 5–8.
46. Crouch, S. P., K. J. Slater, and J. Fletcher. 1992. Regulation of cytokine release from mononuclear cells by the iron-binding protein lactoferrin. *Blood* 80: 235–240.
47. He, S., A. R. McEuen, S. A. Blewett, P. Li, M. G. Buckley, P. Leufkens, and A. F. Walls. 2003. The inhibition of mast cell activation by neutrophil lactoferrin: uptake by mast cells and interaction with tryptase, chymase and cathepsin G. *Biochem. Pharmacol.* 65: 1007–1015.
48. Vukusic, S., M. Hutchinson, M. Hours, T. Moreau, P. Cortinovis-Tourniaire, P. Adeleine, C. Confavreux, and The Pregnancy In Multiple Sclerosis Group. 2004. Pregnancy and multiple sclerosis (the PRIMS study): clinical predictors of post-partum relapse. *Brain* 127: 1353–1360.
49. Gee, K., M. Kryworuchko, and A. Kumar. 2004. Recent advances in the regulation of CD44 expression and its role in inflammation and autoimmune diseases. *Arch. Immunol. Ther. Exp.* 52: 13–26.
50. Brocke, S., C. Piercy, L. Steinman, I. L. Weissman, and T. Veromaa. 1999. Antibodies to CD44 and integrin α4, but not L-selectin, prevent central nervous system inflammation and experimental encephalomyelitis by blocking secondary leukocyte recruitment. *Proc. Natl. Acad. Sci. USA* 96: 6896–6901.
51. Laman, J. D., C. B. M. Maassen, M. M. Schellekens, L. Visser, M. Kap, E. de Jong, M. van Puijenbroek, M. J. van Stipdonk, M. van Meurs, C. Schwärzler, and U. Günthert. 1998. Therapy with antibodies against CD40L (CD154) and CD44-variant isoforms reduces experimental autoimmune encephalomyelitis induced by a proteolipid protein peptide. *Mult. Scler.* 4: 147–153.
52. Verdrengh, M., R. Holmdahl, and A. Tarkowski. 1995. Administration of antibodies to hyaluronanreceptor (CD44) delays the start and ameliorates the severity of collagen II arthritis. *Scand. J. Immunol.* 42: 353–358.
53. ten Bokum, A. M., L. J. Hofland, and P. M. van Hagen. 2000. Somatostatin and somatostatin receptors in the immune system: a review. *Eur. Cytokine Netw.* 11: 161–176.
54. Onuki, M., M. M. Ayers, C. C. Bernard, and J. M. Orian. 2001. Axonal degeneration is an early pathological feature in autoimmune-mediated demyelination in mice. *Microsc. Res. Tech.* 52: 731–739.
55. Lassmann, H., W. Bruck, and C. Lucchinetti. 2001. Heterogeneity of multiple sclerosis pathogenesis: implications for diagnosis and therapy. *Trends Mol. Med.* 7: 115–121.
56. Lucchinetti, C. F., J. Parisi, and W. Bruck. 2005. The pathology of multiple sclerosis. *Neurol Clin.* 23: 77–105.